Sensor fault diagnosis in inland navigation networks based on a grey-box model

P. Segovia [*,**,***] **J. Blesa** [**] **E. Duviella** [***] **L. Rajaoarisoa** [***]
F. Nejjari [*] **V. Puig** [*,**]

[*] *Research Center for Supervision, Safety and Automatic Control (CS2AC), Universitat Politècnica de Catalunya (UPC), Terrassa Campus, Gaia Building, Rambla Sant Nebridi 22, 08222 Terrassa, Spain {pablo.segovia, fatiha.nejjari, vicenc.puig}@upc.edu*
[**] *Institut de Robòtica i Informàtica Industrial (CSIC-UPC), c/ Llorens i Artigas 4-6, 08028 Barcelona, Spain {joaquim.blesa@upc.edu}*
[***] *IMT Lille Douai, Univ. Lille, Unité de Recherche Informatique Automatique, F-59000 Lille, France {eric.duviella, lala.rajaoarisoa}@imt-lille-douai.fr*

Abstract: Inland navigation networks are equipped with limnimeters to measure and record water level data for the control of water levels and the management of water resources. When faults occur on sensors, corrupted data can be considered as correct, leading to undesirable management actions. Therefore, it is necessary to detect and localize these faults. In this paper, the detection and localization of sensor faults is performed through the analysis of the parameters of a grey-box model, which are obtained from available real data. The parameters are determined with a sliding window, with the exception of the delays, which are considered known *a priori*. A fault is detected and then localized when there is a change in the value of the parameters. This approach is well suited for constant faults and particularly well adapted for intermittent faults. Data of an inland navigation reach located in the north of France are used to highlight the performance of the proposed approach.

Keywords: Large-scale systems, inland waterways, fault diagnosis, grey-box model.

1. INTRODUCTION

Inland waterways are large-scale systems that run through France with a total length of approximately 6000 *km*. These networks are usually decomposed into reaches to simplify their study. A reach is defined as a part of the network between two locks, and is generally equipped with controlled gates to regulate the water levels by dispatching volumes of water. Indeed, in order to accommodate the navigation of vessels, it is necessary that the level of each reach be within a certain interval around a setpoint known as the Normal Navigation Level (NNL). The design and implementation of control algorithms such as those proposed in Segovia et al. (2017); Rajaoarisoa et al. (2014); Horváth et al. (2014c) require the measurement of levels, which is achieved by means of limnimeters. However, the level measurements can be corrupted by several types of faults, which can lead to undesired control actions. Thus, fault detection and isolation (FDI) techniques must be designed to detect and localize the faults.

Fault diagnosis in water systems has attracted considerable attention, which has fostered the proposal of many approaches and techniques. Blesa et al. (2010) proposed a fault detection method based on a linear parameter-varying (LPV) model in order to detect faults that occur in open-channel systems. Bedjaoui and Weyer (2011) carried out a comparison of detection methods based on residual generation, extended Kalman filters and finite memory observers to detect and localize leaks in an irrigation network. Nabais et al. (2012) proposed another sensor fault detection approach for irrigation canals based on residual generation. Le Pocher et al. (2012) derived another sensor fault detection method for a real undershot/overshot gate based on physical and black-box models. A finite memory observer was presented by Akhenak et al. (2013) to detect sensor and actuator faults in a dam-gallery system by using a recursive subspace identification method. Horváth et al. (2014a) developed an interval model based on physical equations and a classification algorithm to detect faults on sensors in an inland navigation reach. Hassanabadi et al. (2016) proposed an unknown input observer design for delayed LPV systems represented in the polytopic framework, aiming at detecting and isolating sensor and actuator faults in an open-flow canal. Sensor fault detec-

⋆ This work has been partially funded by the Spanish State Research Agency (AEI) and the European Regional Development Fund (ERFD) through the projects DEOCS (ref. MINECO DPI2016-76493), SCAV (ref. MINECO DPI2017-88403-R) and through the grant IJCI-2014-20801. This work has also been partially funded by AGAUR of Generalitat de Catalunya through the Advanced Control Systems (SAC) group grant (2017 SGR 482). The authors thank the Scientific Research Network GRAISyHM and the Regional Council of Hauts-de-France for their support, and also *Voies Navigables de France* for the data provided, which has made possible this work.

tion methods for inland waterways were designed using the Integrator Delay Zero (IDZ) model (Segovia et al., to appear) and interval models (Blesa et al., 2014), respectively. By using an interval model, it was possible to deal with the uncertainties of the nominal model. The grey-box model of navigation reaches detailed in Horváth et al. (2014b) was coupled with a classification algorithm to detect abrupt and incipient sensor faults in Duviella et al. (2013). These approaches were well-suited to detect abrupt and incipient faults, but are not dedicated to intermittent faults.

In this work, a grey-box model is used to estimate the water levels of navigation reaches by considering a sliding window. The quality of the model is checked by means of fitting indicators. Then, validity intervals are determined for each parameter of the grey-box model. When a sensor fault occurs, the value of the identified parameters is modified. If the value of one parameter crosses the predefined boundaries of its validity interval, a fault is detected and isolated. This FDI approach is designed to consider constant and intermittent faults, and is then tested by considering the Cuinchy-Fontinettes reach (CFr) located in the north of France.

The paper is organized as follows: Section 2 presents the grey-box model. The description of the FDI approach is given in Section 3. Section 4 presents the case study and the data used to illustrate the fault detection approach. Section 5 draws conclusions and outlines future steps.

2. GREY-BOX MODEL

The grey-box modeling approach proposed in Horváth et al. (2014b) is summarized herein by considering an additional assumption: each actuator is equipped with one limnimeter. The structure of the model is a first order plus time delay for every input/output pair:

$$\hat{\boldsymbol{y}}_{k+1} = \boldsymbol{A}\overline{\boldsymbol{y}}_{k|\tau} + \boldsymbol{B}\overline{\boldsymbol{u}}_{k|\tau} \tag{1}$$

with matrices $\boldsymbol{A} \in \mathbb{R}^{n\times n^2}$ and $\boldsymbol{B} \in \mathbb{R}^{n\times n^2}$. The input variables $\overline{\boldsymbol{u}}_{k|\tau} \in \mathbb{R}^{n^2\times 1}$ correspond to a combination of the components of the input vector $\boldsymbol{u}_k$=$[u_k^1 \dots u_k^n]^T$ with convenient delays, where $u_k^l = Q_k^l \ \forall l = 1, ..., n$ are the different discharges along the canal. Similarly, the output variables $\overline{\boldsymbol{y}}_{k|\tau} \in \mathbb{R}^{n^2\times 1}$ correspond to a combination of the components of the output vector $\boldsymbol{y}_k$=$[y_k^1 \dots y_k^n]^T$ with convenient delays, where $y_k^i = L_k^i \ \forall i = 1, ..., n$ are the different level measurements along the canal (*see* Fig. 1). The matrix $\boldsymbol{\tau} \in \mathbb{N}^{n\times n}$ given in Eq. (2) gathers the time delays between the measurement points L^i and L^j, and also between the discharge Q^i and the measurement point L^j, respectively. For instance, the runtime from i to j is given by $\tau_{i,j} \in \mathbb{N}$. It is worth noting that $\boldsymbol{\tau}$ is not symmetric, as the upstream and downstream wave velocities are different.

$$\boldsymbol{\tau} = \begin{bmatrix} 0 & \tau_{1,2} & \cdots & \tau_{1,n} \\ \tau_{2,1} & 0 & \ddots & \vdots \\ \vdots & \ddots & 0 & \tau_{n-1,n} \\ \tau_{n,1} & \cdots & \tau_{n,n-1} & 0 \end{bmatrix} \tag{2}$$

The time delays are determined according to the well-known relations given in Litrico and Fromion (2004).

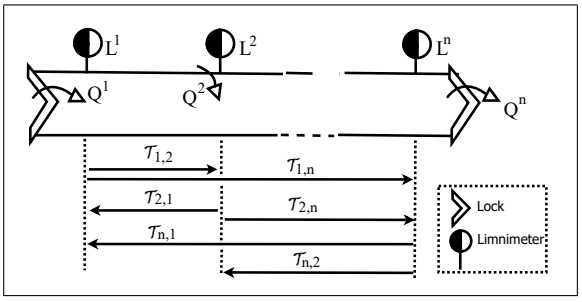

Fig. 1. Time delays $\tau_{i,j}$ between each pair of measurement points.

The vector $\overline{\boldsymbol{y}}_{k|\tau}$ is expressed as

$$\overline{\boldsymbol{y}}_{k|\tau} = \begin{bmatrix} \overline{\boldsymbol{y}}_{k|\tau}^1 \ \overline{\boldsymbol{y}}_{k|\tau}^2 \ \cdots \ \overline{\boldsymbol{y}}_{k|\tau}^n \end{bmatrix}^T, \tag{3}$$

with $\overline{\boldsymbol{y}}_{k|\tau}^i = \begin{bmatrix} L_{k-\tau_{i,1}}^1 \ L_{k-\tau_{i,2}}^2 \ \cdots \ L_{k-\tau_{i,n}}^n \end{bmatrix}$.

Likewise, $\overline{\boldsymbol{u}}_{k|\tau}$ reads as

$$\overline{\boldsymbol{u}}_{k|\tau} = \begin{bmatrix} \overline{\boldsymbol{u}}_{k|\tau}^1 \ \overline{\boldsymbol{u}}_{k|\tau}^2 \ \cdots \ \overline{\boldsymbol{u}}_{k|\tau}^n \end{bmatrix}^T, \tag{4}$$

with $\overline{\boldsymbol{u}}_{k|\tau}^i = \begin{bmatrix} Q_{k-\tau_{i,1}}^1 \ Q_{k-\tau_{i,2}}^2 \ \cdots \ Q_{k-\tau_{i,n}}^n \end{bmatrix}$.

Matrix $\boldsymbol{A}$ is defined as the direct sum of the $1-by-n$ vectors $\boldsymbol{A}^i$, *i.e.* $\boldsymbol{A}$= $\bigoplus_{i=1}^n \boldsymbol{A}^i$ ($\boldsymbol{B}$ is expressed similarly):

$$\boldsymbol{A} = \begin{bmatrix} \boldsymbol{A}^1 & \boldsymbol{0_n} & \cdots & \boldsymbol{0_n} \\ \boldsymbol{0_n} & \boldsymbol{A}^2 & \ddots & \vdots \\ \vdots & \ddots & \ddots & \boldsymbol{0_n} \\ \boldsymbol{0_n} & \cdots & \boldsymbol{0_n} & \boldsymbol{A}^n \end{bmatrix} \tag{5}$$

with $\boldsymbol{A}^i = \begin{bmatrix} a^{i,1} & \cdots & a^{i,n} \end{bmatrix}$ and $\boldsymbol{0_n}$ the $1-by-n$ zero vector. Note that $a^{i,i}$ is the parameter that links $\hat{y}_{k+1}^i$ to y_k^i with no delay.

Equation (1) is rewritten as follows:

$$\hat{\boldsymbol{y}}_{k+1} = \boldsymbol{M}\ \boldsymbol{\Phi}_k \tag{6}$$

Considering the block-diagonal structure of matrices $\boldsymbol{A}$ and $\boldsymbol{B}$, the i-th level $\hat{y}_{k+1}^i$ can be estimated as

$$\hat{y}_{k+1}^i = \boldsymbol{M}^i\ \boldsymbol{\Phi}_k^i\ , \tag{7}$$

with $\boldsymbol{M}^i = \begin{bmatrix} \boldsymbol{A}^i \ \boldsymbol{B}^i \end{bmatrix}$ and $\boldsymbol{\Phi}_k^i = \begin{bmatrix} \overline{\boldsymbol{y}}_{k|\tau}^i \ \overline{\boldsymbol{u}}_{k|\tau}^i \end{bmatrix}^T$.

Then, $\boldsymbol{M}^i$ is the solution of the linear least squares problem. N samples of the measured discharges Q_k^i and levels L_k^i are considered in its computation:

$$\boldsymbol{M}^i = \boldsymbol{Y}^i \ \left(\overline{\boldsymbol{\Phi}}^i\right)^T \ \left(\overline{\boldsymbol{\Phi}}^i \ \left(\overline{\boldsymbol{\Phi}}^i\right)^T\right)^{-1}\ , \tag{8}$$

with $\boldsymbol{Y}^i = \begin{bmatrix} y_{\chi+1}^i \ \cdots \ y_N^i \end{bmatrix}$, $\overline{\boldsymbol{\Phi}}^i = \begin{bmatrix} \boldsymbol{\Phi}_\chi^i \ \cdots \ \boldsymbol{\Phi}_{N-1}^i \end{bmatrix}$, and $\chi = \max(\boldsymbol{\tau}) + 1$, where $\max(\boldsymbol{\tau})$ is the maximum entry of matrix $\boldsymbol{\tau}$ given in (2).

The following fit coefficients are used to determine the accuracy of the model with respect to the measurements:

- *Pearson product-moment correlation coefficient* measures the linear dependence between two variables:

$$R^i = \frac{\sum_{k=1}^{N} \left(y_k^i - \lambda_{y^i}\right)\left(\hat{y}_k^i - \lambda_{\hat{y}^i}\right)}{\sqrt{\sum_{k=1}^{N} \left(y_k^i - \lambda_{y^i}\right)^2}\sqrt{\sum_{k=1}^{N} \left(\hat{y}_k^i - \lambda_{\hat{y}^i}\right)^2}} \quad (9)$$

with λ_{y^i} and $\lambda_{\hat{y}^i}$ the mean value of measured and estimated water levels, respectively. This coefficient is bounded between +1 (total positive linear correlation) and -1 (total negative linear correlation), and 0 means that there is no linear correlation.

- *Nash-Sutcliffe model efficiency coefficient* is used to assess the predictive power of hydrological models (Nash and Sutcliffe, 1970):

$$E^i = 1 - \frac{\sum_{k=1}^{N} \left(y_k^i - \hat{y}_k^i\right)^2}{\sum_{k=1}^{N} \left(y_k^i - \lambda_{y^i}\right)^2} \quad (10)$$

E^i can range from 1 to $-\infty$, where 1 indicates a perfect match of modeled and observed values, 0 corresponds to the case in which the model predictions are as accurate as the mean of observed data and $E^i < 0$ means that the model predictions are less accurate than the mean of observed data. It can also be expressed in percent when its value is positive.

Once the proposed model is validated, the grey-box model and the coefficients of matrices $\boldsymbol{A}$ and $\boldsymbol{B}$ can be used to design the FDI strategy.

3. FAULT DIAGNOSIS

The fault diagnosis is focused on sensor level faults:

$$L_k^i = L_k^{i,0} + \Delta_k^i, \quad \forall i = 1, ..., n \quad (11)$$

where $L_k^{i,0}$ denotes the level i and Δ_k^i the fault at time k.

As model (1) provides the level estimations $\hat{\boldsymbol{y}}_{k+1}$, the most straightforward fault detection method consists in evaluating the difference between the level sensor measurements and the estimations:

$$r_k^i = y_k^i - \hat{y}_k^i, \quad \forall i = 1, ..., n \quad (12)$$

where r_k^i is the temporal residual of the i-th level sensor. The fault detection test can be formulated as follows:

$$\phi_k^{r^i} = \begin{cases} 0 \text{ if } r_k^i \in [\underline{\sigma}^i, \overline{\sigma}^i] \Rightarrow \text{ No Fault} \\ 1 \text{ otherwise} \end{cases} \quad (13)$$

where bounds $\underline{\sigma}^i$ and $\overline{\sigma}^i$ are the maximum positive and negative deviations of the residual r_k^i in a fault-free scenario, respectively.

Another possibility consists in considering the evolution of the grey-box parameters. To do so, the determination of $\boldsymbol{M}^i$ given in Eq. (8) is performed by considering a time window of size N_w. Hence, a temporal matrix $\boldsymbol{M}_k^i$ is computed at every instant k:

$$\boldsymbol{M}_k^i = \boldsymbol{Y}_k^i \left(\overline{\boldsymbol{\Phi}}_k^i\right)^T \left(\overline{\boldsymbol{\Phi}}_k^i \left(\overline{\boldsymbol{\Phi}}_k^i\right)^T\right)^{-1}, \quad (14)$$

with $\boldsymbol{Y}_k^i = [y_{k+\chi+1-N_w}^i \cdots y_k^i]$, $\overline{\boldsymbol{\Phi}}_k^i = [\boldsymbol{\Phi}_{k+\chi-N_w}^i \cdots \boldsymbol{\Phi}_{k-1}^i]$.

The parameters $a_k^{j,i}$ and $b_k^{j,i}$ $\forall i, j = 1...n$ are obtained from $\boldsymbol{M}_k^i = [\boldsymbol{A}_k^i \ \boldsymbol{B}_k^i]$. The next step consists in comparing these parameters with their bounds $[\underline{a^{j,i}}, \overline{a^{j,i}}]$ and $[\underline{b^{j,i}}, \overline{b^{j,i}}]$ obtained in a fault-free scenario which is representative enough and validated by means of fitting indicators (9)–(10). Finally, the parameter fault signals $\phi_k^{a^{j,i}}$ and $\phi_k^{b^{j,i}}$ can be generated in a similar way as $\phi_{r_k^i}$ in (13):

$$\phi_k^{a^{j,i}} = \begin{cases} 0 \text{ if } a_k^{j,i} \in [\underline{a^{j,i}}, \overline{a^{j,i}}] \Rightarrow \text{ no fault} \\ 1 \text{ otherwise} \end{cases} \quad (15)$$

$\phi_k^{b^{j,i}}$ is computed as $\phi_k^{a^{j,i}}$ but considering the parameter estimations $b_k^{j,i}$ and the bounds $[\underline{b^{j,i}}, \overline{b^{j,i}}]$ in (15). The main drawback of the fault detection test defined in (15) is that a non-persistent excitation in the inputs when applying (14) can lead to false alarms due to parameter estimation errors. To overcome this issue, the parameter fault signals $\phi_k^{a^{j,i}}$ and $\phi_k^{b^{j,i}}$ should be computed only when the input persistent exciting order is enough to guarantee an accurate parameter estimation (Ljung, 1999).

A fault is detected when at least one fault signal $\phi_k^{r^i}$, $\phi_k^{a^{j,i}}$ or $\phi_k^{b^{j,i}}$ is activated (its value equals 1). Once the fault is detected, it should be isolated with the information of the different fault signals. The main problem of isolating level faults defined in (11) considering model (3) is that, since every level is present in all level estimations, every level fault potentially affects all the fault signals (residual fault signals and parameter fault signals). This means that it is not possible to isolate faults by means of the standard Boolean fault signature matrix (Gertler, 1998). However, as the effect of a level fault in the limnimeter L^i (Δ_k^i) in the estimation of the level in the limnimeter L^j ($\hat{y}_k^j$) is delayed by $\tau_{i,j}$, $\boldsymbol{\tau}$ can be used to isolate faults considering the fault signature occurrence and delay as proposed in Puig and Blesa (2013). For instance, when a fault Δ_k^i occurs, the temporal residual fault signal $\phi_k^{r^i}$ and the parametric fault signals $\phi_k^{a^{j,i}}$ and $\phi_k^{b^{j,i}}$ $\forall i = 1, \cdots, n$ should be activated in the first place. In the case of parametric fault signals, the effect of the fault Δ_k^i is more direct in the estimation of parameter $a_k^{i,i}$. Due to the use of a time window of length N_w, an extra delay between the fault appearance and the effect in the fault signals can be present. Next, the effect of the fault will be propagated to the nearest measurement point j, which will affect the estimation of the level and the parameters. As the effect of the fault Δ_k^i is attenuated in the propagation, it might be observed only in the nearest measurement points.

4. CASE STUDY

4.1 Description of the system

The Cuinchy-Fontinettes reach (CFr) has been particularly studied in the last years due to its importance in the inland waterway management in the north of France. It is equipped with two main locks (the Cuinchy lock upstream and the Fontinettes lock downstream), two controlled gates (the Cuinchy gate beside the Cuinchy lock and the gate *Porte de Garde* at Aire-sur-la -Lys (*see* Fig. 2) and three limnimeters that allow measuring the level at Cuinchy (L^C), Aire-sur-la-Lys (L^A) and Fontinettes (L^F) with a sampling time $T_s = 1\ min$. The controlled discharges are applied by means of the Cuinchy lock and gate

(Q^C), the *Porte de Garde* gate (Q^A) and the Fontinettes lock (Q^F). These magnitudes are measured each 15 *min* and then oversampled every minute.

The CFr is 42 *km* long, with the gate *Porte de Garde* located 28 *km* downstream of Cuinchy. In addition, this reach is characterized by a negligible slope along its course. Therefore, its dynamics are impacted by strong resonance phenomena and large time delays. Lock operations create waves that travel back and forth along the reach during several hours until their attenuation. The large distances that the waves travel along the reach result in delays.

The navigation is allowed from 6:30 *am* to 8:30 *pm* (Monday-Saturday), and from 9 *am* to 6 *pm* on Sundays, with a lower navigation demand. Waves are created during these periods of time, and their attenuation takes place during the night, outside the navigation schedule.

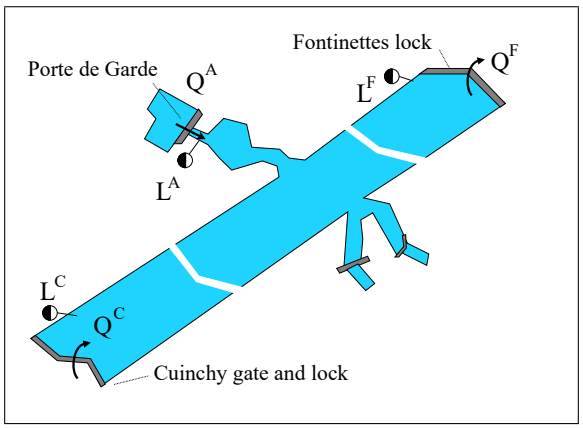

Fig. 2. Schematics of the CFr.

The occurrence of faults in limnimeters can have a strong impact on the inland waterways management. At the lower management scale, the navigation might be required to stop since the control of the water levels is done by considering wrong data. At the higher management scale, the water resources might not be adequately dispatched. These issues constitute the main motivations of FDI in inland navigation reaches. The faults may not only be a consequence of an artificial measurement offset during several hours (constant faults) but also due to transmission problems (intermittent faults).

The grey-box modeling and FDI approach are used to detect and isolate sensor faults by considering real data from the CFr, namely from October 30, 2013 (Thursday) to November 17, 2013 (Sunday). Part of these data are used to compute the parameters of the grey-box model and determine the validity intervals of its main parameters. The remaining data are used to test the approach by introducing artificial faults.

4.2 Grey-box model

Real data from the limnimeters and discharges are re-synchronized by considering a sampling time of one minute. Then, the delays between each part of the CFr are estimated according to the characteristics of the system and considering $Q_{max} = 0.6\ m^3/s$ as the average discharge. These values are stored in a matrix of delays as follows (the values are in minutes):

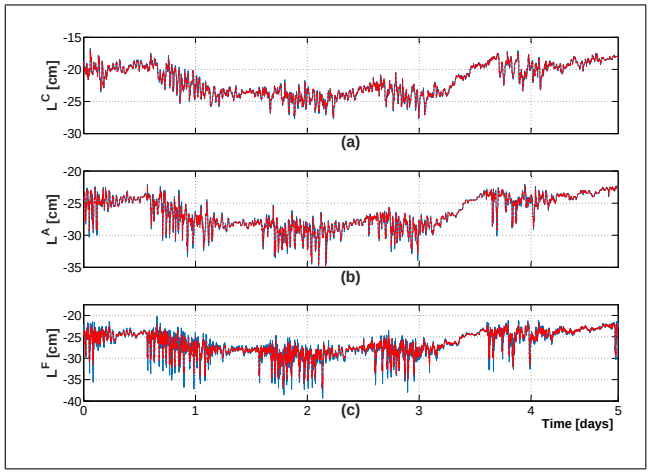

Fig. 3. Water levels in: (a) Cuinchy. (b) Aire-sur-la-Lys. (c) Fontinettes. Measured levels: blue solid line; estimated levels: red solid line.

$$\boldsymbol{\tau} = \begin{bmatrix} 0 & 78 & 115 \\ 79 & 0 & 37 \\ 116 & 37 & 0 \end{bmatrix} \tag{16}$$

According to these delays, the input and output vectors $\overline{\boldsymbol{u}}_{k|\tau} \in \mathbb{R}^{9\times 1}$ and $\overline{\boldsymbol{y}}_{k|\tau} \in \mathbb{R}^{9\times 1}$ are built by considering the following inputs and outputs: $u_k^1 = Q_k^C$, $y_k^1 = L_k^C$ for Cuinchy; $u_k^2 = Q_k^A$, $y_k^2 = L_k^A$ for Aire-sur-la-Lys; and $u_k^3 = Q_k^F$, $y_k^3 = L_k^F$ for Fontinettes.

The vectors $\overline{\boldsymbol{u}}_{k|\tau}$ and $\overline{\boldsymbol{y}}_{k|\tau}$ are used in the parameter identification of the model by considering a sliding window of size $N_w = 1440\ min$ (1 day). This allows taking into account the CFr dynamics during night and day, thus guaranteeing the input persistent exciting order condition.

By considering five consecutive days from the first day, October 30, 2013 (Thursday), a model for each window is identified. This model is used to estimate the levels $\hat{L}_k^i$ as outputs of the grey-box model. The real measurements L_k^i and the estimated $\hat{L}_k^i$ are depicted in Fig. 3 in blue and dashed red lines, respectively, for each of the three limnimeters. Note that these values are relative to the NNL (equal to 3.8 *m* for the CFr), and therefore the values L_k^i=0 correspond to the NNL in Figs. 3 and 5 (same for $\hat{L}_k^i$).

The grey-box parameters change for each window. Fig. 4 depicts this evolution for the $a_k^{i,i}$ terms. The Nash-Sutcliffe (E^i) and correlation (R^i) coefficients are also computed to verify the quality of the model. These coefficients are depicted in Fig. 4(d) for the limnimeter L^C and are in the interval [80, 100] %, which means that the model predictions are accurate with regard to the real data. The average values of these coefficients for the three limnimeters are given in Table 1.

Table 1. Average values of Nash-Sutcliffe (E^i) and correlation (R^i) coefficients

Limnimeter	E^i [%]	R^i [%]
L^C	90	95
L^A	87	93
L^F	76	87

Based on these data, the intervals for the $a_k^{i,i}$ parameters are determined. They are depicted as black dashed lines in Fig. 4(a), 4(b) and 4(c). These intervals will be used to detect and isolate faults.

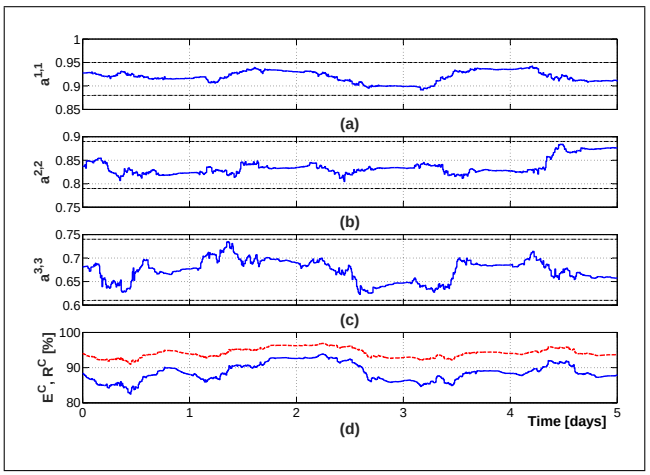

Fig. 4. Values of the $a_k^{i,i}$ parameters and determined thresholds: (a) $a^{1,1}$. (b) $a^{2,2}$. (c) $a^{3,3}$. (d) R^C (red solid line) and E^C (blue solid line).

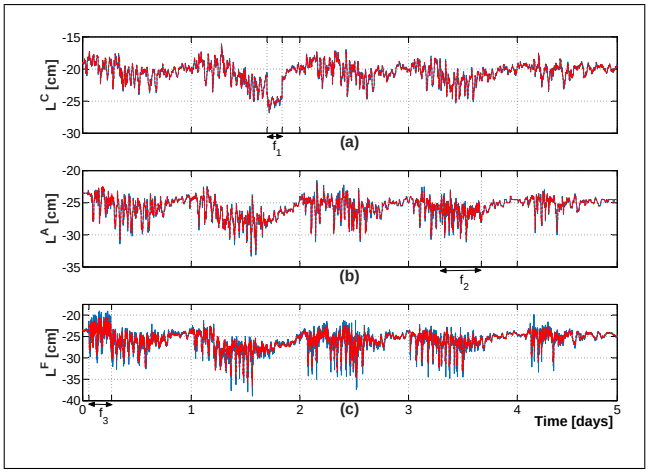

Fig. 5. Water levels in: (a) Cuinchy. (b) Aire-sur-la-Lys. (c) Fontinettes. Measured levels (impacted by faults): blue solid line; estimated levels: red solid line.

4.3 FDI in limnimeters

The measurements corresponding to five consecutive days starting from November 12, 2013 (Tuesday) have been considered in order to create three faulty scenarios by adding three faults to the real measurements. Fault f_1 corresponds to a constant fault of -8 *cm* on the level L^C. Fault f_2 consists in an intermittent fault with a magnitude of 1.5 *cm* on the level L^A. Fault f_3 is also an intermittent fault with a magnitude of 5 *cm* on the level L^F. The features of the three faults are summarized in Table 2.

The three measured levels and their estimations are depicted in Fig. 5 in blue and red dashed lines, respectively, for the three limnimeters. The time occurrence and the duration of the faults are indicated with black arrows. Due to the dynamics of the CFr and the occurrence of lock operations, the detection of the faults is not obvious.

The water level residuals have also been computed (*see* Fig. 6). It is not possible to detect fault f_1 (*see* Fig. 6(a)), except for two peaks in r^C that appear when the constant fault occurs and disappears. Moreover, the magnitude of these two peaks is not higher than other peaks in the residual r^C. By considering f_2 and residual r^A (*see* Fig. 6(b)), an increase in the frequency of peaks with a similar magnitude can be observed during the occurrence of the fault, but their magnitude is not big enough. A similar behavior is obtained for f_3 and residual r^F (*see* Fig. 6(c)).

The proposed FDI approach is performed according to the identified grey-box parameters by considering the $a_k^{i,i}$ terms and the predefined thresholds given in Fig. 6. These terms change during the simulation, as it is shown in Fig. 7. The parameter $a^{1,1}$ crosses the upper threshold after the occurrence of the fault f_1, which allows detecting the occurrence of one fault. The isolation is done by considering which parameter is impacted. Here, the fault f_1 is isolated because the limnimeter L^C is impacted. The detection and isolation of faults f_2 and f_3 is achieved by considering the parameters $a^{2,2}$ and $a^{3,3}$, respectively. The faults are detected when these parameters cross one of the predefined interval bounds. It can be observed that all faults can be detected after 4 *h* in average, and only the parameter residual fault signals $\phi_k^{a^{j,i}}$ are activated. The detection delays, given in Table 3, are due to the size of the sliding window. However, the magnitude of the considered faults is very small: larger faults should be detected faster and activate more fault signals.

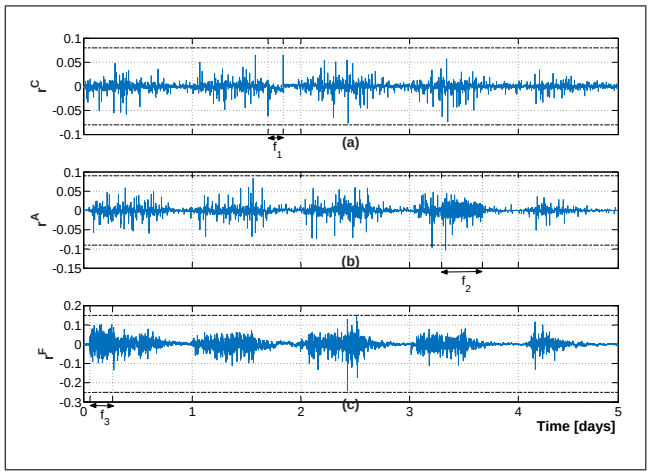

Fig. 6. Water level residuals (blue solid line) and thresholds (black dashed lines) for: (a) Cuinchy. (b) Aire-sur-la-Lys. (c) Fontinettes.

It is shown that the detection and isolation of constant and intermittent faults can be performed by dealing with the grey-box model parameters. The dynamics of the system are modified in each scenario, but only one parameter moves away from its nominal value. Thus, this approach seems well suited to diagnose this kind of faults.

Table 2. Considered faults

Fault	Mag. [*cm*]	Occurrence (dd:hh:mm)	Duration [*min*]
f_1	-8	01:16:44	200
f_2	1.5	03:07:04	540
f_3	5	00:01:24	300

Table 3. Detection delay of each fault

Fault	Detection delay $[min]$
f_1	241
f_2	261
f_3	239

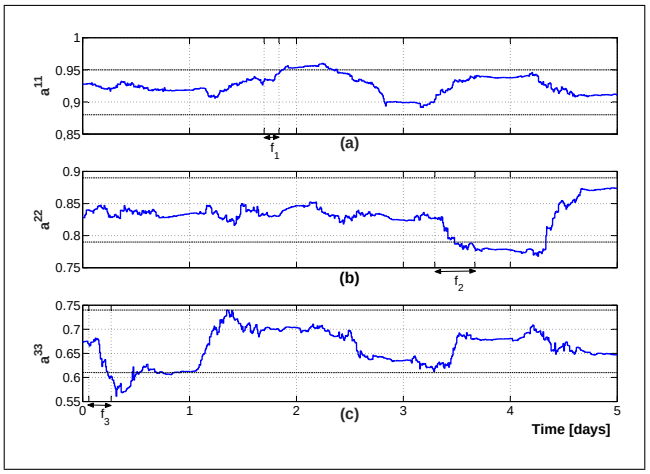

Fig. 7. Value of the $a_k^{i,i}$ parameters (blue solid line) and determined thresholds (black dashed lines) in the faulty case: (a) $a^{1,1}$, (b) $a^{2,2}$, (c) $a^{3,3}$.

5. CONCLUSION

In this paper, a sensor fault diagnosis that aims at detecting and isolating constant and intermittent faults is proposed. It is based on a grey-box model designed for free-surface water canals, *i.e.* their surface is in contact with the air in the atmosphere. The coefficients of this model are estimated according to real measurements, except for the *a priori* known time delays. The supervision of the model parameter values leads to the detection and isolation of faults when these values cross one of the predefined thresholds. The proposed approach is tested by means of real measurements obtained from the sensors available at the CFr. Three faulty scenarios have been used to highlight the performance of the proposed approach.

Future steps derived from this work will look at the effect of multiple sensor faults. In addition, a recursive identification method of the grey-box coefficients will also be developed with the purpose of decreasing the fault detection time. Finally, a fault-tolerant control scheme aiming at satisfying the management objectives in presence of faults will be developed.

REFERENCES

Akhenak, A., Duviella, E., Bako, L., and Lecoeuche, S. (2013). Online fault diagnosis using recursive subspace identification: Application to a dam-gallery open channel system. *Control Engineering Practice*, 21, 797–806.

Bedjaoui, N. and Weyer, E. (2011). Algorithms for leak detection, estimation, isolation and localization in open channels. *Control Engineering Practice*, 19, 564–573.

Blesa, J., Horváth, K., Duviella, E., Puig, V., Bolea, Y., Rajaoarisoa, L., and Chuquet, K. (2014). Model-based sensor supervision in inland navigation networks: Cuinchy-Fontinettes case study. *Journal of Maritime Research*, 11(2), 81–88.

Blesa, J., Puig, V., and Bolea, Y. (2010). Fault detection using interval LPV models in an open-flow canal. *Control Engineering Practice*, 18, 460–470.

Duviella, E., Rajaoarisoa, L., Blesa, J., and Chuquet, K. (2013). Fault detection and isolation of inland navigation channel: Application to the Cuinchy-Fontinettes reach. In *52nd IEEE Conference on Decision and Control, Florence, Italy, December 10-13*, 4877–4882.

Gertler, J. (1998). Fault detection and diagnosis in engineering systems. *Publisher: Dekker*.

Hassanabadi, A.H., Shafiee, M., and Puig, V. (2016). UIO design for singular delayed LPV systems with application to actuator fault detection and isolation. *International Journal of Systems Science*, 47, 107–121.

Horváth, K., Blesa, J., Duviella, E., Rajaoarisoa, L., Puig, V., and Chuquet, K. (2014a). Sensor fault diagnosis of inland navigation system using physical model and pattern recognition approach. *IFAC Proceedings Volumes*, 47(3), 5309–5314. 19th IFAC World Congress.

Horváth, K., Duviella, E., Blesa, J., Rajaoarisoa, L., Bolea, Y., Puig, V., and Chuquet, K. (2014b). Grey-box model of inland navigation channel: application to the Cuinchy-Fontinettes reach. *Journal of Intelligent Systems*, 23(2), 183–199.

Horváth, K., Duviella, E., Petreczky, M., Rajaoarisoa, L., and Chuquet, K. (2014c). Model Predictive Control of water levels in a navigation canal affected by resonance waves. *HIC 2014, New York, USA, 17-21 August*.

Le Pocher, O., Duviella, E., Bako, L., and Chuquet, K. (2012). Sensor fault detection of a real undershot/overshot gate based on physical and nonlinear black-box models. *IFAC Proceedings Volumes*, 45(20), 1083–1088.

Litrico, X. and Fromion, V. (2004). Simplified modeling of irrigation canals for controller design. *Journal of Irrigation and Drainage Engineering*, 130, 373–383.

Ljung, L. (1999). *System identification : theory for the user (2nd Edition)*. Prentice Hall, Upper Saddle River.

Nabais, J.L., Mendonça, L.F., and Botto, M.A. (2012). Sensor fault tolerant architecture for irrigation canals. *10th Portuguese Conference on Automatic Control 16-18 July 2012, CONTROLO2012, Funchal, Portugal*.

Nash, J.E. and Sutcliffe, J.V. (1970). River flow forecasting through conceptual models part I: a discussion of principles. *Journal of Hydrology*, 10(3), 282–290.

Puig, V. and Blesa, J. (2013). Limnimeter and rain gauge FDI in sewer networks using an interval parity equations based detection approach and an enhanced isolation scheme. *Control Engineering Practice*, 21(2), 146–170.

Rajaoarisoa, L., Horváth, K., Duviella, E., and Chuquet, K. (2014). Large-scale system control based on decentralized design. Application to Cuinchy Fontinette reach. *IFAC Proceedings Volumes*, 47(3), 11105–11110.

Segovia, P., Rajaoarisoa, L., Nejjari, F., Puig, V., and Duviella, E. (2017). Decentralized control of inland navigation networks with distributaries: application to navigation canals in the north of France. In *American Control Conference (ACC), 2017*, 3341–3346. IEEE.

Segovia, P., Blesa, J., Horváth, K., Rajaoarisoa, L., Nejjari, F., Puig, V., and Duviella, E. (to appear). Modeling and fault diagnosis of flat inland navigation canals. *Proceedings of the Institution of Mechanical Engineers, Part I: Journal of Systems and Control Engineering*. doi:10.1177/0959651818773187.